Mathematical Modelling of Engineering Problems
Vol. 11, No. 2, February, 2024, pp. 464-476
Journal homepage: http://iieta.org/journals/mmep

SH-Wave Propagation in Functionally Graded Magneto-Electro-Elastic Substrate at Irregular Boundaries

Hemalatha Kulandhaivel, Santosh Kumar*

Department of Mathematics, College of Engineering and Technology, SRM Institute of Science and Technology, Kattankulathur 603203, India

Corresponding Author Email: santoshh@srmist.edu.in

https://doi.org/10.18280/mmep.110218

Received: 25 July 2023
Revised: 22 October 2023
Accepted: 30 October 2023
Available online: 27 February 2024

Keywords:
functional gradient, magneto-electro-elastic material, irregular interface, point source, wave number, phase velocity, inhomogeneity, perturbation

ABSTRACT

The current study examines the behavior of an SH wave traveling over a functionally graded magneto-elastic substrate arrangement. At the substrate-vacuum interface, two irregularities with different shapes—rectangular and parabolically shaped—are considered in electrically and magnetically open cases and electrically and magnetically short cases. A study is also done on the combined impact of inhomogeneity, depth source, and irregularity. With the help of the Fourier transform, inverse Fourier transform, and perturbation technique, complex frequency relation has been derived for each type of irregular interface. The results' key characteristics are highlighted. In order to know the impact of the parameters involved, a particular model consisting of $BaTiO_3$-$CoFe_2O_4$ magneto-electro-elastic material has been taken. The findings were presented in the form of graphs, which were created using Mathematica 7. Graphs are plotted for variations in wavenumber and phase velocity. This calculation model could be the ideal match for laminated FGMEE structures utilized as surface acoustic wave devices since the variation of the film's magneto-electromechanical characteristics changes gradually with depth and throughout the production process (SAW). As a result, it can serve as a theoretical foundation for the design of high-performance SAW devices.

1. INTRODUCTION

In contrast to the approach to piezoelectric or piezomagnetic material, magneto-electro-elastic (MEE) materials have both piezoelectric and piezomagnetic characteristics, particularly with the electromagnetic coupling effect. A brand-new kind of intelligent material known as functionally graded magneto-electro-elastic material (FGMEE) features inhomogeneous mechanical properties, a composition that gradually changes in one direction, and the ability to convert between magnetic electric and mechanical energy precisely. Smart gadgets, including sensors, actuators, and electromagnetic memory components, frequently use this new kind of intelligent composite material. The design of these devices could be substantially aided by having a general grasp of them. Compared to the static analysis literature, studies on the transient properties of FGMEE structures are incredibly underrepresented. Therefore, there is a pressing need to study the quick reactions of such structures to enhance their performance. As a result, many individuals are very interested in the research on wave propagation in MEE and FGMEE materials. Van Suchtelen [1] created the first artificial magneto-electro-elastic material artificially by mixing piezoelectric and piezomagnetic materials. According to Van Run et al. [2], the $BaTiO_3$-$CoFe_2O_4$ composite they created had the most potent electromagnetic effect available at the time. Later, Bracke and Van Vliet discovered a broad magneto-electric transducer made of composite material [3]. Inhomogeneity issues with magneto-electro-elastic multi-inclusions and their applications in composite materials were encountered by Li [4]. Green's function for anisotropic magnetoelastic solids having an oval cavity or a crack was covered by Liu et al. [5]. Authors such as Pan and Han [6], Bhangake and Ganesan [7], and Huang et al. [8] discussed the functionally graded MEE materials using various solutions methods. Wave propagation on magneto-electro-elastic multilayered plates was observed by Chen et al. [9] In MEE Materials, Arman [10] investigated twelve shear surface waves steered by clamped or unconstrained limits. Surface electro-elastic SH waves in a layered device with a piezoelectric substrate and a hard dielectric layer were described by Danoyan and Piliposian [11]. Li and Wei [12, 13] encountered the pre-stressed and MEE solids' impact on the surface wave speed and velocity of FGMEE materials. In their study, Wu et al. [14] used the modified Pagano approach to analyze the three-dimensional static behavior of FGMEE plates. Anisotropic FGMEE beams exposed to arbitrary loading were the focus of a static analysis study by Huang et al. [15]. Zhao and Chen [16] discussed using the symplectic framework for plane research for FGMEE materials. Chen et al. [17] noticed wave propagation with a nonlocal influence in MEE multilayered plates. Yang et al. [18] talked about applying analytical and finite element methods to analyze the natural properties of multilayered magneto-electro-elastic

plates. Vinyas [19] covered the computational analysis of intelligent magneto-electro-elastic materials and structures. To represent the propagation of elastodynamic waves in composites made of elastic, piezoelectric, and magneto-electro-elastic materials, Othmani et al. [20] used orthogonal polynomial methods. In a magneto-electro-elastic layered structure with such a non-perfect and locally perturbed interface, Chaki and Bravo-Castillero [21] investigated the statistical modeling of anti-plane surface waves.

Seismology, civil engineering, and mechanical engineering all benefit from understanding the propagation and scattering of waves in granular and medium materials. It is also apparent that structural abnormalities in the wave propagation medium impact it. Many academics have taken into account uneven borders of specific shapes and sizes to keep the solution process mathematically simple. It is possible to name a few essential works on wave propagation in a medium with irregular boundaries. Chattopadhyay et al. [22] explained how SH waves go through a crooked monoclinic crustal layer. When Singh [23] reached a layered medium with erratic boundary surfaces, he came upon the love wave. Singh and Chattopadhyay [24] briefed about how magnetoelastic shear waves go through an unruly layer of self-reinforcement. The scattering of a Love wave traveling in an uneven anisotropy porous stratum under initial load was covered by Chattaraj et al. [25]. Love type wave propagation in an uneven piezoelectric structure, Singh et al. [26]. Regarding the effect of irregularities on the SH-type direction of propagation inside the micropolar elasticity composite structure, Singh et al. [27] came across some comments. Love-type waves in the couple-stress stratum that were ill-bonded to an uneven viscous substrate were discussed by Ray and Singh [28]. The effects of piezoelectricity and reinforcement on the propagation of SH waves in irregularly layered, inadequately bonded FGPM structures were explored by Chaki and Singh [29]. The Love-type wave propagation case-wise analysis was encountered by Gupta et al. [30] in an unsteady fissured porous stratum covered in sand. The features of SH wave scattering and propagation in simplified Cosserat isotropic layered structures at irregular borders were explored by Chaki and Singh [31].

Chaki et al. [32] discussed the effects of rectangular/parabolic-shaped irregularities on the propagation of shear horizontal waves in a slightly compressible layered structure. In functionally graded piezo-poroelastic mediums with electrode boundaries and suddenly thickened imperfect interface, Singh et al. [33] analytical analysis of Love wave propagation was encountered. In functionally graded fracturing porous sedimentary with interfacial irregularity, Gupta et al. [34] investigated the flexoelectric influence on SH-wave propagation. Love wave propagation in an isotropic fluid-saturated porous material under the influence of parabolic irregularity was discussed by Saini and Poonia [35]. According to Bhat and Manna [36], the reinforcing, porosity distributions, non-local elasticity, and uneven boundary surfaces all affect the behaviour of Love-wave fields. Singh et al. [37] studied the scattering processes of Love-type wave propagation in a multilayer porous piezoelectric structure with surface irregularity. Kumari and Srivastava [38] studied the torsional wave in void-type porous layers using parabolic irregularity in viscoelastic and piezoelectric media. Willis's [39] formula for expanding an integral as a series and Tranter's [40] Integral Transforms in Mathematical Physics are used in mathematical calculations. Up to now, no attempt has been made to study the propagation of SH waves in an irregularly functionally graded magneto-electro-elastic substrate.

Due to the widespread use of functionally graded materials in our daily lives, numerous research projects have been done and are ongoing. Functionally graded materials are utilized in developing and manufacturing SAW devices, communications devices, SAW filters for Global Positioning Systems (GPS), and mobile phones. These applications motivated us to continue our research on functionally graded materials, particularly in functionally graded magneto-electro-elastic mediums, and we did so after [29, 31, 32]. The current study examines the behavior of an SH wave traveling over a functionally graded magneto-elastic substrate arrangement. At the substrate-vacuum interface, two irregularities with different shapes—rectangular and parabolically shaped—are considered in electrically and magnetically open cases and electrically and magnetically short cases. A study is also done on the combined impact of inhomogeneity, depth source, and irregularity. The variable separation method was used to arrive at the dispersion equations for the propagation of the SH wave. With the help of the Fourier transform, inverse Fourier transform, and perturbation technique, complex frequency relation has been derived for each type of irregular interface [29]. The results' key characteristics are highlighted. In order to know the impact of the parameters involved, a particular model consisting of $BaTiO_3$-$CoFe_2O_4$ magneto-electro-elastic material has been taken. Graphs are plotted for variations in wavenumber and phase velocity. This calculation model could be the ideal match for laminated FGMEE structures utilized as surface acoustic wave devices since the variation of the film's magneto-electromechanical characteristics changes gradually with depth and throughout the production process (SAW). As a result, it can serve as a theoretical foundation for the design of high-performance SAW devices.

2. BASIC EQUATIONS AND NOTATIONS

We investigate an SH-wave that passes through an uneven magneto-electro-elastic substrate with typical wave velocity *c* and wave number *k*. Two different situations of irregularity in the shapes of a rectangular and a parabola are considered. The origination *O* is considered the midway of the selected irregularities in Figure

s 1 and 2, which shows a graphic of the layer structure under consideration. The irregularity's maximum depth and span are *H* and 2*s*, respectively. Let *S* represent the location of the disturbance's source along the x-axis and *l* distance from the origin. A time-harmonic disturbance is produced by the source at *S*.

The interface equations for irregularities with rectangular and parabolic shapes can be written as

$$x = \varepsilon h(y) = \begin{cases} 0 & \text{for } |y| > s, \\ H & \text{for } |y| \le s, \end{cases} \tag{1}$$

$$x = \varepsilon h(y) = \begin{cases} 0 & \text{for } |y| > s, \\ H\left(1 - \dfrac{y^2}{s^2}\right) & \text{for } |y| \le s, \end{cases} \tag{2}$$

where, $\varepsilon = \frac{H}{2s} \ll 1$ is the perturbation parameter, which is presumable to be small.

This assumption is reinforced by the earth's surface model,

where an irregularity's depth H is frequently minor in comparison to its span 2s.

Let (u, v, w) represent a particle's displacement components in (x, y, z) directions, respectively. The z-axis does not affect the displacement or potential electrical components since the SH wave only causes displacement in the z-direction and propagates in the y-direction. As a result, we can calculate the mechanical displacement components and the electric and magnetic potentials are

$$u = 0,\ v = 0,\ w = w(x, y, t), \phi = \phi(x, y, t),\ \psi = \psi(x, y, t) \tag{3}$$

The following are governing equations of motion for static behavior with unrestricted electric charges and no body forces:

$$\left.\begin{aligned} T_{ij,j} &= \rho \ddot{u}_i \\ D_{i,i} &= 0 \\ B_{i,i} &= 0 \end{aligned}\right\} \tag{4}$$

The dot shows differentiation in time, the comma shows differentiation in space, and the repeating index in the subscript shows summation.

The following is the relation between displacement and strain components:

$$S_{ij} = \frac{1}{2}\left(u_{ij} + u_{ji}\right) \tag{5}$$

Quasi-static approximation of the Maxwell equations yields:

$$E_i = -\phi_{,i} \quad \text{and} \quad H_i = -\psi_{,i} \tag{6}$$

For a transversely isotropic medium with the z-axis being the symmetric axis and the poling axis of the magneto-electro-elastic material, the constitutive equations are

$$\left.\begin{aligned} T_{11} &= C_{11}S_{11} + C_{12}S_{22} + C_{13}S_{33} - e_{31}E_3 - h_{31}H_3 \\ T_{22} &= C_{12}S_{11} + C_{11}S_{22} + C_{23}S_{33} - e_{32}E_3 - h_{32}H_3 \\ T_{33} &= C_{13}S_{11} + C_{13}S_{22} + C_{33}S_{33} - e_{33}E_3 - h_{33}H_3 \\ T_{23} &= 2C_{44}S_{23} - e_{15}E_2 - h_{15}H_2 \\ T_{31} &= 2C_{44}S_{31} - e_{15}E_1 - h_{15}H_1 \\ T_{12} &= \left(C_{44} - C_{12}\right)S_{12} \\ D_1 &= 2e_{15}S_{31} + \kappa_{11}E_1 + \beta_{11}H_1 \\ D_2 &= 2e_{15}S_{23} + \kappa_{11}E_2 + \beta_{11}H_2 \\ D_3 &= e_{31}S_{11} + e_{31}S_{22} + e_{33}S_{33} + \kappa_{33}E_3 + \beta_{33}H_3 \\ B_1 &= 2h_{15}S_{31} + \beta_{11}E_1 + \mu_{11}H_1 \\ B_2 &= 2h_{15}S_{23} + \beta_{11}E_2 + \mu_{11}H_2 \\ B_3 &= h_{31}S_{11} + h_{31}S_{22} + h_{33}S_{33} + \beta_{33}E_3 + \mu_{33}H_3 \end{aligned}\right\} \tag{7}$$

In the specified direction, the component magnetic field and electric field are represented by the gradients of a magneto potential and electric potential for a space variable.

The nonvanishing equations derived from Eqs. (3), (4), and (7) apply to the propagation of the SH wave,

$$\left.\begin{aligned} T_{31,1} + T_{23,2} &= \rho \ddot{w} \\ D_{1,1} + D_{2,2} &= 0 \\ B_{1,1} + B_{2,2} &= 0 \end{aligned}\right\} \tag{8}$$

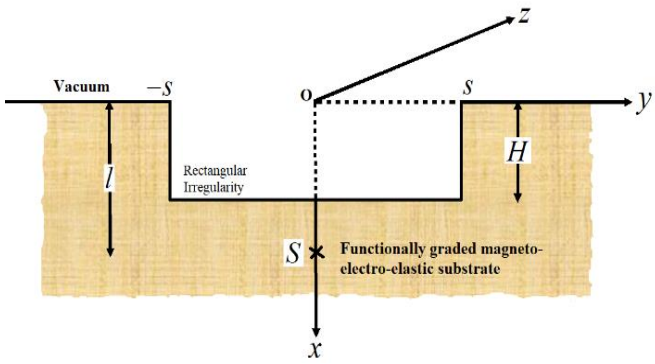

Figure 1. The problem of rectangular irregularity in geometry

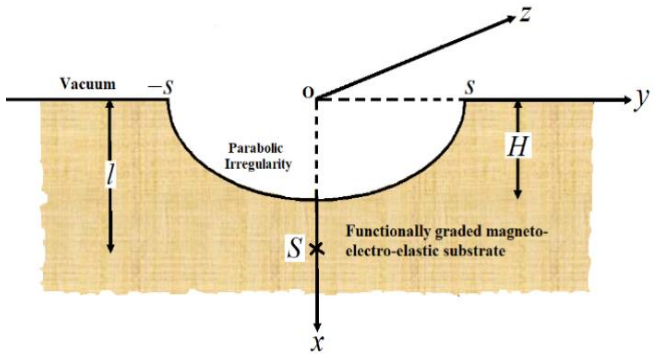

Figure 2. The problem of parabolic irregularity in geometry

3. DYNAMICS OF THE PROBLEM

3.1 Dynamics of FGMEE substrate

Eq. (8) can be used to derive the motion equations for the SH wave propagating along the x-axis as

$$\left.\begin{aligned} &C_{44}^{(1)}\nabla^2 w + e_{15}^{(1)}\nabla^2\phi + h_{15}^{(1)}\nabla^2\psi + C_{44}^{(1)}\frac{\partial w}{\partial x} + e_{15}^{(1)}\frac{\partial \phi}{\partial x} + h_{15}^{(1)}\frac{\partial \psi}{\partial x} = \rho_1\frac{\partial^2 w}{\partial t^2} \\ &e_{15}^{(1)}\nabla^2 w - \kappa_{11}^{(1)}\nabla^2\phi - \beta_{11}^{(1)}\nabla^2\psi + e_{15}^{(1)}\frac{\partial w}{\partial x} - \kappa_{11}^{(1)}\frac{\partial \phi}{\partial x} - \beta_{11}^{(1)}\frac{\partial \psi}{\partial x} = 0 \\ &h_{15}^{(1)}\nabla^2 w - \beta_{11}^{(1)}\nabla^2\phi - \mu_{11}^{(1)}\nabla^2\psi + h_{15}^{(1)}\frac{\partial w}{\partial x} - \beta_{11}^{(1)}\frac{\partial \phi}{\partial x} - \mu_{11}^{(1)}\frac{\partial \psi}{\partial x} = 0 \end{aligned}\right\} \tag{9}$$

The FGMEE substrate material characteristics are expected to be positively exponentially distributed across the depth (x-axis). The FGMEE substrate functional gradients are therefore regarded as

$$\left.\begin{aligned} &C_{44}^{(1)}(x) = C_{44}^{(01)}e^{\alpha x}, e_{15}^{(1)}(x) = e_{15}^{(01)}e^{\alpha x}, h_{15}^{(1)}(x) = h_{15}^{(01)}e^{\alpha x}, \\ &\kappa_{11}^{(1)}(x) = \kappa_{11}^{(01)}e^{\alpha x}, \beta_{11}^{(1)}(x) = \beta_{11}^{(01)}e^{\alpha x}, \mu_{11}^{(1)}(x) = \mu_{11}^{(01)}e^{\alpha x}, \\ &\rho_1 = \rho^0 e^{\alpha x} \end{aligned}\right\} \tag{10}$$

Employing Eq. (10) in Eq. (9) we get

$$\left.\begin{aligned} &C_{44}^{(01)}\left(\nabla^2 w + \alpha\frac{\partial w}{\partial x}\right) + e_{15}^{(01)}\left(\nabla^2\phi + \alpha\frac{\partial \phi}{\partial x}\right) + h_{15}^{(01)}\left(\nabla^2\psi + \alpha\frac{\partial \psi}{\partial x}\right) = \rho^0\frac{\partial^2 w}{\partial t^2} \\ &e_{15}^{(01)}\left(\nabla^2 w + \alpha\frac{\partial w}{\partial x}\right) - \kappa_{11}^{(01)}\left(\nabla^2\phi + \alpha\frac{\partial \phi}{\partial x}\right) - \beta_{11}^{(01)}\left(\nabla^2\psi + \alpha\frac{\partial \psi}{\partial x}\right) = 0 \\ &h_{15}^{(01)}\left(\nabla^2 w + \alpha\frac{\partial w}{\partial x}\right) - \beta_{11}^{(01)}\left(\nabla^2\phi + \alpha\frac{\partial \phi}{\partial x}\right) - \mu_{11}^{(01)}\left(\nabla^2\psi + \alpha\frac{\partial \psi}{\partial x}\right) = 0 \end{aligned}\right\} \tag{11}$$

From Eq. (11), we see that w, ϕ, and ψ are coupled. By introducing two new functions

$$\phi' = \phi - \mathrm{m}w;\ \psi' = \psi - \mathrm{n}w \tag{12}$$

Substitution of Eq. (12) into Eq. (11) yields,

$$\left.\begin{aligned} &\nabla^2 w + \alpha\frac{\partial w}{\partial x} - \frac{1}{c^2}\frac{\partial^2 w}{\partial t^2} = 0\\ &\nabla^2\phi' + \alpha\frac{\partial \phi'}{\partial x} = 0\\ &\nabla^2\psi' + \alpha\frac{\partial \psi'}{\partial x} = 0 \end{aligned}\right\} \tag{13}$$

where,

$$c = \sqrt{\frac{\overline{C_{44}^{(01)}}}{\rho^0}},\ \mathrm{m} = \frac{\mu_{11}^{(01)}e_{15}^{(01)} - \beta_{11}^{(01)}h_{15}^{(01)}}{\kappa_{11}^{(01)}\mu_{11}^{(01)} - \left(\beta_{11}^{(01)}\right)^2},\ \mathrm{n} = \frac{\kappa_{11}^{(01)}h_{15}^{(01)} - \beta_{11}^{(01)}e_{15}^{(01)}}{\kappa_{11}^{(01)}\mu_{11}^{(01)} - \left(\beta_{11}^{(01)}\right)^2},$$

$$\overline{C_{44}^{(01)}} = C_{44}^{(01)} + \frac{\mu_{11}^{(01)}\left(e_{15}^{(01)}\right)^2 + \kappa_{11}^{(01)}\left(h_{15}^{(01)}\right)^2 - 2\beta_{11}^{(01)}e_{15}^{(01)}h_{15}^{(01)}}{\kappa_{11}^{(01)}\mu_{11}^{(01)} - \left(\beta_{11}^{(01)}\right)^2}.$$

Then, the stress tensor, electric displacement vector, and magnetic induction vector in Eq. (7) can be expressed in terms of

$$\left.\begin{aligned} &T_{11} = T_{33} = T_{12} = 0,\ D_3 = 0, B_3 = 0,\\ &T_{23} = e^{\alpha x}\left(\overline{C_{44}^{(01)}}w_{,2} + e_{15}^{(01)}\phi'_{,2} + h_{15}^{(01)}\psi'_{,2}\right),\\ &T_{13} = e^{\alpha x}\left(\overline{C_{44}^{(01)}}w_{,1} + e_{15}^{(01)}\phi'_{,1} + h_{15}^{(01)}\psi'_{,1}\right),\\ &D_1 = \left(-\kappa_{11}^{(01)}\phi'_{,1} - \beta_{11}^{(01)}\psi'_{,1}\right),\\ &D_2 = \left(-\kappa_{11}^{(01)}\phi'_{,2} - \beta_{11}^{(01)}\psi'_{,2}\right),\\ &B_1 = \left(-\beta_{11}^{(01)}\phi'_{,1} - \mu_{11}^{(01)}\psi'_{,1}\right),\\ &B_2 = \left(-\beta_{11}^{(01)}\phi'_{,2} - \mu_{11}^{(01)}\psi'_{,2}\right) \end{aligned}\right\} \tag{14}$$

The solutions of Eq. (13) convert when the time-harmonic dependency of SH wave propagation is assumed as

$$\left.\begin{aligned} &w = W(x,y)e^{i\omega t}\\ &\phi' = \Phi'(x,y)e^{i\omega t}\\ &\psi' = \Psi'(x,y)e^{i\omega t} \end{aligned}\right\} \tag{15}$$

It is to be noted that SH wave velocity is lesser than that of a substrate. In light of Eq. (15), Eq. (13) reduces to the following

$$\left.\begin{aligned} &\nabla^2 W + \alpha\frac{\partial W}{\partial x} + \frac{\omega^2}{c^2}W = 0\\ &\nabla^2\Phi' + \alpha\frac{\partial \Phi'}{\partial x} = 0\\ &\nabla^2\Psi' + \alpha\frac{\partial \Psi'}{\partial x} = 0 \end{aligned}\right\} \tag{16}$$

In general, we define the following Fourier transforms as

$$\overline{f}(x,\eta) = \int_{-\infty}^{\infty} f(x,y)e^{i\eta y}dy \tag{17}$$

and the subsequent inverse Fourier transform is defined as

$$f(x,y) = \frac{1}{2\pi}\int_{-\infty}^{\infty}\overline{f}(x,\eta)e^{-i\eta y}d\eta \tag{18}$$

Taking the Fourier transforms for Eq. (16) now, we discover

$$\left.\begin{aligned} &\nabla^2\overline{W} + \alpha\frac{d\overline{W}}{dx} + \left(\frac{\omega^2}{c^2} - \eta^2\right)\overline{W} = 0\\ &\frac{d^2\overline{\Phi}'}{dx^2} - \eta^2\overline{\Phi}' + \alpha\frac{d\overline{\Phi}'}{dx} = 0\\ &\frac{d^2\overline{\Psi}'}{dx^2} - \eta^2\overline{\Psi}' + \alpha\frac{d\overline{\Psi}'}{dx} = 0 \end{aligned}\right\} \tag{19}$$

With the aid of Eqs. (17)-(19) may be expressed for FGMEE substrate as

$$\left.\begin{aligned} &\overline{W} = Ae^{-r_1 x}\\ &\overline{\Phi}' = Be^{-r_2 x}\\ &\overline{\Psi}' = Ce^{-r_2 x} \end{aligned}\right\} \tag{20}$$

where, A, B, C are unknown constants, $r_1 = \frac{\alpha + \sqrt{\alpha^2 + 4\frac{\omega^2}{l^2}}}{2}$ and $r_2 = \frac{\alpha + \sqrt{\alpha^2 - 4\eta^2}}{2}$.

Now, required solutions of FGMEE substrate Eq. (20) becomes

$$\left.\begin{aligned} &\overline{W} = Ae^{-r_1 x}\\ &\overline{\Phi} = Be^{-r_2 x} + \mathrm{m}Ae^{-r_1 x}\\ &\overline{\Psi} = Ce^{-r_2 x} + \mathrm{n}Ae^{-r_1 x} \end{aligned}\right\} \tag{21}$$

Therefore, mechanical displacement and electric potential function in FGMEE substrate as

$$\left.\begin{aligned} &w = \frac{1}{2\pi}\int_{-\infty}^{\infty}\left(Ae^{-r_1 x} + \frac{2}{r_1}e^{r_1 x}e^{-r_1 l}\right)e^{-i\eta y}d\eta\\ &\phi = \frac{1}{2\pi}\int_{-\infty}^{\infty}\left(Be^{-r_2 x} + \mathrm{m}Ae^{-r_1 x}\right)e^{-i\eta y}d\eta\\ &\psi = \frac{1}{2\pi}\int_{-\infty}^{\infty}\left(Ce^{-r_2 x} + \mathrm{n}Ae^{-r_1 x}\right)e^{-i\eta y}d\eta \end{aligned}\right\} \tag{22}$$

where, the existence of the source within the FGMEE substrate causes the second term, as in the integrand of W, to be introduced.

3.2 Dynamics of FGMEE vacuum

Air's dielectric constant κ_0 and μ_0 vary substantially from the dielectric constant of piezoelectric materials. As a result,

the piezoelectric layer's upper surface is often exposed to air. Therefore, the electric and magnetic potential functions φ_v and ψ_v may be considered a vacuum for air in the region.

$$\nabla^2\phi_v = 0, \nabla^2\psi_v = 0 \tag{23}$$

The electric and magnetic displacement components of a vacuum are described as follows

$$\begin{aligned} D_v &= -\kappa_0 \frac{\partial \phi_v}{\partial x}, \\ B_v &= -\mu_0 \frac{\partial \psi_v}{\partial x} \end{aligned} \tag{24}$$

Eq. (23) solutions convert when the time-harmonic dependency of SH wave propagation is assumed as

$$\phi = \Phi(x,y)e^{i\omega t},\ \psi = \Psi(x,y)e^{i\omega t} \tag{25}$$

Approaching in a similar fashion, and taking the Fourier transform of Eq. (23), we result in

$$\Phi_v = De^{r_3 x},\ \Psi_v = Ee^{r_3 x} \tag{26}$$

where, D and E are unknown constants. And $r_3 = \eta$.

Therefore, the solution for the vacuum may be instated as

$$\left.\begin{aligned} \phi_v &= \frac{1}{2\pi}\int_{-\infty}^{\infty}\left(De^{r_3 x}\right)e^{-i\eta y}d\eta \\ \psi_v &= \frac{1}{2\pi}\int_{-\infty}^{\infty}\left(Ee^{r_3 x}\right)e^{-i\eta y}d\eta \end{aligned}\right\} \tag{27}$$

4. BOUNDARY CONDITIONS

The adhesion to the following permissible boundary conditions is enforced to identify the frequency equations of SH wave:

1) Mechanical tractions at the irregular interface continuity, that is $x = \varepsilon h(y)$

$$T_{31} - \varepsilon h'(y)T_{23} = 0 \tag{28}$$

2) Electrical boundary condition at $x = \varepsilon h(y)$

(i) Electrically open case:

$$D_1 = D_v \tag{29}$$

$$\phi = \phi_v \tag{30}$$

(ii) Electrically short case:

$$\phi = 0 \tag{31}$$

3) Magnetic boundary condition at $x = \varepsilon h(y)$

(i) Magnetically open case:

$$B_1 = B_v \tag{32}$$

$$\psi = \psi_v \tag{33}$$

(ii) Magnetically short case:

$$\psi = 0 \tag{34}$$

5. SOLUTION TREATMENT

The arbitrary variables *A, B, C, D,* and *E* are considered functions of the perturbation parameter because the substrate and vacuum interface is irregular. Expanding the constants (*A, B, C, D, E*) in powers of ε and neglecting quadratic and higher powers of ε, we approximate the constants as [29]

$$\begin{gathered} A \cong A_0 + A_1\varepsilon, B \cong B_0 + B_1\varepsilon, C \cong C_0 + C_1\varepsilon, \\ D \cong D_0 + D_1\varepsilon, E \cong E_0 + E_1\varepsilon. \end{gathered}$$

For a very small value of ε, we may also agree to the following approximations:

$$\begin{aligned} &e^{\pm\vartheta\varepsilon h} \cong 1 \pm \vartheta\varepsilon h, \\ &\cos(\vartheta\varepsilon h) \cong 1, \\ &\sin(\vartheta\varepsilon h) \cong \vartheta\varepsilon h \end{aligned}$$

where, ϑ can be any value. Now, with the helps from Eqs. (14), (22), we arrive at the following from boundary condition (28),

$$\begin{aligned} &\int_{-\infty}^{\infty}\Big\{-\left(1+\alpha\varepsilon h(y)\right)\Big[\overline{C_{44}^{(01)}}r_1\left(A_0+A_1\varepsilon\right)\left(1-r_1\varepsilon h(y)\right) \\ &+2C_{44}^{(01)}\left(1+r_1\varepsilon h(y)\right)e^{-r_1 l}+e_{15}^{(01)}r_2\left(B_0+B_1\varepsilon\right)\left(1-r_2\varepsilon h(y)\right) \\ &+h_{15}^{(01)}r_2\left(C_0+C_1\varepsilon\right)\left(1-r_2\varepsilon h(y)\right)\Big]\Big\}e^{-i\eta y}d\eta \\ &-\varepsilon\int_{-\infty}^{\infty}\left(1+\alpha\varepsilon h(y)\right)\Big[\overline{C_{44}^{(01)}}r_1\left(A_0+A_1\varepsilon\right)\left(1-r_1\varepsilon h(y)\right) \\ &+C_{44}^{(01)}\frac{2}{r_1}\left(1+r_1\varepsilon h(y)\right)e^{-r_1 l}+e_{15}^{(01)}r_2\left(B_0+B_1\varepsilon\right)\left(1-r_2\varepsilon h(y)\right) \\ &+h_{15}^{(01)}r_2\left(C_0+C_1\varepsilon\right)\left(1-r_2\varepsilon h(y)\right)\Big]h'(y)e^{-i\eta y}d\eta = 0 \end{aligned} \tag{35}$$

Now, let us define the Fourier transform of $h(y)$ as

$$\bar{h}(\lambda) = \int_{-\infty}^{\infty} h(y)e^{i\lambda y}dy \tag{36}$$

and the subsequent inverse transform is defined as

$$h(y) = \frac{1}{2\pi}\int_{-\infty}^{\infty}\bar{h}(\lambda)e^{-i\lambda y}d\lambda \tag{37}$$

Therefore, it may be derived that

$$h'(y) = \frac{-i}{2\pi}\int_{-\infty}^{\infty}\lambda\bar{h}(\lambda)e^{-i\lambda y}d\lambda \tag{38}$$

In light of Eq. (37), Eq. (35) is transformed into

$$\frac{\varepsilon}{2\pi}\int_{-\infty}^{\infty}\left\{\int_{-\infty}^{\infty}\left[\overline{C_{44}^{(01)}}r_1^2A_0-2C_{44}^{(01)}r_1e^{-r_1l}+e_{15}^{(01)}r_2^2B_0+h_{15}^{(01)}r_2^2C_0\right.\right.$$
$$-\alpha\overline{C_{44}^{(01)}}r_1A_0-\alpha e_{15}^{(01)}r_2B_0-2\alpha C_{44}^{(01)}e^{-r_1l}-\alpha h_{15}^{(01)}r_2C_0$$
$$\left.\left.-\overline{C_{44}^{(01)}}\lambda\eta A_0-e_{15}^{(01)}\lambda\eta B_0-h_{15}^{(01)}\lambda\eta C_0\right]\right\}\bar{h}(\lambda)e^{-i(\lambda+\eta)y}d\eta\,d\lambda \quad (39)$$
$$=\int_{-\infty}^{\infty}\left\{\overline{C_{44}^{(01)}}r_1\left(A_0+A_1\varepsilon\right)+e_{15}^{(01)}r_2\left(B_0+B_1\varepsilon\right)\right.$$
$$\left.+2C_{44}^{(01)}e^{-r_1l}+h_{15}^{(01)}r_2\left(C_0+C_1\varepsilon\right)\right\}e^{-i\eta y}d\eta$$

Now, considering the inner integral in the left-hand side of Eq. (39) where λ may be treated as a constant, leads to $d\eta = dk$ [29]. Further, by replacing η by k on the right-hand side of Eq. (39) and using Eq. (37), we obtain

$$\overline{C_{44}^{(01)}}r_1\left(A_0+A_1\varepsilon\right)+e_{15}^{(01)}r_2\left(B_0+B_1\varepsilon\right)$$
$$+2C_{44}^{(01)}e^{-r_1l}+h_{15}^{(01)}r_2\left(C_0+C_1\varepsilon\right)=\varepsilon P_1(k) \quad (40)$$

where,

$$P_1(k)=\frac{1}{2\pi}\int_{-\infty}^{\infty}\left[\overline{C_{44}^{(01)}}\left(r_1^2-\alpha r_1-\lambda\eta\right)A_0-2C_{44}^{(01)}\left(r_1-\alpha\right)e^{-r_1l}\right.$$
$$\left.+e_{15}^{(01)}\left(r_2^2-\alpha r_2-\lambda\eta\right)B_0+h_{15}^{(01)}\left(r_2^2-\alpha r_2-\lambda\eta\right)C_0\right]^{\eta=k-\lambda}\bar{h}(\lambda)d\lambda \quad (41)$$

Approaching in a similar fashion, boundary conditions (29)-(34), we obtain

$$\kappa_{11}^{(01)}r_2\left(B_0+B_1\varepsilon\right)+\beta_{11}^{(01)}r_2\left(C_0+C_1\varepsilon\right)+\kappa_0r_3\left(D_0+D_1\varepsilon\right)=\varepsilon P_2(k) \quad (42)$$

$$\mathrm{m}\left(A_0+A_1\varepsilon\right)+B_0+B_1\varepsilon-D_0-D_1\varepsilon=\varepsilon P_4(k) \quad (43)$$

$$\mathrm{m}\left(A_0+A_1\varepsilon\right)+B_0+B_1\varepsilon=\varepsilon P_6(k) \quad (44)$$

$$\beta_{11}^{(01)}r_2\left(B_0+B_1\varepsilon\right)+\mu_{11}^{(01)}r_2\left(C_0+C_1\varepsilon\right)+\mu_0r_3\left(E_0+E_1\varepsilon\right)=\varepsilon P_3(k) \quad (45)$$

$$\mathrm{n}\left(A_0+A_1\varepsilon\right)+C_0+C_1\varepsilon-E_0-E_1\varepsilon=\varepsilon P_5(k) \quad (46)$$

$$\mathrm{n}\left(A_0+A_1\varepsilon\right)+C_0+C_1\varepsilon=\varepsilon P_7(k) \quad (47)$$

where,

$$P_2(k)=\frac{1}{2\pi}\int_{-\infty}^{\infty}\left[-\alpha r_2\kappa_{11}^{(01)}B_0-\alpha r_2\beta_{11}^{(01)}C_0\right.$$
$$\left.+\kappa_{11}^{(01)}r_2^2B_0+\beta_{11}^{(01)}r_2^2C_0-\kappa_0r_3D_0\right]^{\eta=k-\lambda}\bar{h}(\lambda)d\lambda \quad (48)$$

$$P_3(k)=\frac{1}{2\pi}\int_{-\infty}^{\infty}\left[-\alpha r_2\beta_{11}^{(01)}B_0-\alpha r_2\mu_{11}^{(01)}C_0\right.$$
$$\left.+\beta_{11}^{(01)}r_2^2B_0+\mu_{11}^{(01)}r_2^2C_0-\mu_0r_3E_0\right]^{\eta=k-\lambda}\bar{h}(\lambda)d\lambda \quad (49)$$

$$P_4(k)=\frac{1}{2\pi}\int_{-\infty}^{\infty}\left[r_2B_0+r_1\mathrm{m}A_0+r_3D_0\right]^{\eta=k-\lambda}\bar{h}(\lambda)\,d\lambda \quad (50)$$

$$P_5(k)=\frac{1}{2\pi}\int_{-\infty}^{\infty}\left[r_2C_0+r_1\mathrm{n}A_0+r_3E_0\right]^{\eta=k-\lambda}\bar{h}(\lambda)\,d\lambda \quad (51)$$

$$P_6(k)=\frac{1}{2\pi}\int_{-\infty}^{\infty}\left[r_2B_0+r_1\mathrm{m}A_0\right]^{\eta=k-\lambda}\bar{h}(\lambda)\,d\lambda \quad (52)$$

$$P_7(k)=\frac{1}{2\pi}\int_{-\infty}^{\infty}\left[r_2C_0+r_1\mathrm{n}A_0\right]^{\eta=k-\lambda}\bar{h}(\lambda)\,d\lambda \quad (53)$$

Now, equating the absolute terms not containing ε and the coefficients of ε from Eqs. (40), (42)-(47), we obtain

$$\overline{C_{44}^{(01)}}r_1A_0+e_{15}^{(01)}r_2B_0+h_{15}^{(01)}r_2C_0=-2C_{44}^{(01)}e^{-r_1l} \quad (54)$$

$$\overline{C_{44}^{(01)}}r_1A_1+e_{15}^{(01)}r_2B_1+h_{15}^{(01)}r_2C_1=P_1(k) \quad (55)$$

$$\kappa_{11}^{(01)}r_2B_0+\beta_{11}^{(01)}r_2C_0+\kappa_0r_3D_0=0 \quad (56)$$

$$\kappa_{11}^{(01)}r_2B_1+\beta_{11}^{(01)}r_2C_1+\kappa_0r_3D_1=P_2(k) \quad (57)$$

$$\mathrm{m}A_0+B_0-D_0=0 \quad (58)$$

$$\mathrm{m}A_1+B_1-D_1=P_4(k) \quad (59)$$

$$\mathrm{m}A_0+B_0=0 \quad (60)$$

$$\mathrm{m}A_1+B_1=P_6(k) \quad (61)$$

$$\beta_{11}^{(01)}r_2B_0+\mu_{11}^{(01)}r_2C_0+\mu_0r_3E_0=0 \quad (62)$$

$$\beta_{11}^{(01)}r_2B_1+\mu_{11}^{(01)}r_2C_1+\mu_0r_3E_1=P_3(k) \quad (63)$$

$$\mathrm{n}A_0+C_0-E_0=0 \quad (64)$$

$$\mathrm{n}A_1+C_1-E_1=P_5(k) \quad (65)$$

$$\mathrm{n}A_0+C_0=0 \quad (66)$$

$$\mathrm{n}A_1+C_1=P_7(k) \quad (67)$$

On solving the above Eqs. (54)-(59), (62)-(65) for electrically open and magnetically open case (EOMO), we obtain the values of A_0, A_1, B_0, B_1, C_0, C_1,D_0, D_1, E_0, and E_1 which are provided in the Appendix. With the help of values of unknown constants and Eq. (22), the mechanical displacement component of the irregular FGMEE substrate may be expressed as

$$W=\frac{1}{2\pi}\int_{-\infty}^{\infty}\frac{\gamma_1}{\gamma}\left[\left(1+\frac{\varepsilon\gamma_4}{\gamma_1}\right)e^{-r_1l}+\frac{2\gamma}{r_1\gamma_1}e^{r_1x}e^{-r_1l}\right]e^{-i\eta y}d\eta \quad (68)$$

Similar steps can be taken to acquire the mechanically displaced component of the uneven FGMEE substrate for the electrically short and magnetically short case (ESMS)

$$W=\frac{1}{2\pi}\int_{-\infty}^{\infty}\frac{-2C_{44}^{(01)}e^{-r_1l}}{\bar{\gamma}}\left[\left(1+\frac{\varepsilon\bar{\gamma}_1}{-2C_{44}^{(01)}e^{-r_1l}}\right)e^{-r_1l}+\frac{2\bar{\gamma}}{-2C_{44}^{(01)}}e^{r_1x}\right]e^{-i\eta y}d\eta \quad (69)$$

where, $\gamma, \gamma_1, \gamma_4, \bar{\gamma}, \bar{\gamma}_1$ are provided in Appendix.

6. FREQUENCY EQUATION

6.1 Frequency equation for rectangular-shaped irregularity at the interfacial surface for EOMO case

Eq. (36) with aid of Eq. (1) yields

$$\bar{h}(\lambda) = \frac{4s}{\lambda}\sin(\lambda s) \tag{70}$$

Hence,

$$\gamma_4 = \frac{2s}{\pi}\int_{-\infty}^{\infty}\left[\left(\zeta(k-\lambda)+\zeta(k+\lambda)\right]\frac{\sin(\lambda s)}{\lambda}d\lambda\right. \tag{71}$$

with $\zeta(k-\lambda) = [G_1 + G_2 + G_3 + G_4 + G_5]^{\eta=k-\lambda}$, where, the definitions of G_1, G_2, G_3, G_4, G_5 are in the Appendix, and the argument of $\zeta(k-\lambda)$ results from the fact that $\eta + \lambda = k$. Using the asymptotic formula [32, 33] and hating terms with 2/s and more extensive powers of 2/s for large *s*, we obtain

$$\int_{-\infty}^{\infty}\left[\left(\zeta(k-\lambda)+\zeta(k+\lambda)\right]\frac{1}{\lambda}\sin\left(\frac{\lambda s}{2}\right)d\lambda \cong \frac{\pi}{2}\left(2\zeta(k)\right) = \pi\zeta(k)\right. \tag{72}$$

Eq. (71), in the context of Eq. (72), is simplified to

$$\gamma_4 \cong \frac{2s}{\pi}\left(\pi\zeta(k)\right) = \frac{H}{\varepsilon}\zeta(k) \tag{73}$$

Eq. (68) is simplified, with the aid of Eq. (73),

$$W = \frac{1}{2\pi}\int_{-\infty}^{\infty}\left[\left(\frac{\gamma_1 e^{-r_1 x}}{\gamma\left(1-\dfrac{H\zeta(k)}{\gamma_1}\right)}\right)+\frac{2}{r_1}e^{r_1 x}e^{-r_1 l}\right]e^{-iky}dk \tag{74}$$

Here, the contribution of the integrand's poles determines the value of such an integral. We compute the roots of the following expression to get the pole,

$$\gamma\left(1-\frac{H\zeta(k)}{\gamma_1}\right) = 0 \tag{75}$$

The necessary dispersion solution of the SH-wave traveling in rectangular-shaped irregularly for the EOMO condition is represented by Eq. (75) and is the relationship between wave number and frequency.

6.2 Frequency equation for rectangular-shaped irregularity at the interfacial surface for ESMS case

The mechanically displaced element of the irregularly FGMEE substrate for the ESMS situation may be calculated as follows by following the same procedure as in Section 6.1 and using the same asymptotic formulas [32, 33]:

$$W = \frac{1}{2\pi}\int_{-\infty}^{\infty}\left[\left(\frac{-2C_{44}^{(01)}e^{-r_1 l}e^{-r_1 x}}{\bar{\gamma}\left(1+\dfrac{H\zeta'(k)}{2C_{44}^{(01)}e^{-r_1 l}}\right)}\right)+\frac{2}{r_1}e^{r_1 x}e^{-r_1 l}\right]e^{-iky}dk \tag{76}$$

The necessary dispersion solution of the SH wave propagating through a rectangle-shaped irregularity in an interfacial surface for the ESMS condition is given by Eq. (76),

$$\bar{\gamma}\left(1+\frac{H\zeta'(k)}{2C_{44}^{(01)}e^{-r_1 l}}\right) = 0 \tag{77}$$

6.3 Frequency equation for parabolically-shaped irregularity at the interfacial surface for EOMO case

By adding the parabola Eq. (2) to the Eq. (36), we arrive at

$$\bar{h}(\lambda) = \left(\frac{4Hs}{\varepsilon}\right)\frac{\sin(\lambda s)-\lambda s\cos(\lambda s)}{(\lambda s)^3} \tag{78}$$

Again, approaching in a similar manner, with aid of solution (68) and using Eq. (78), we derive that

$$\gamma_4 = \frac{2Hs}{\pi\varepsilon}\int_{-\infty}^{\infty}\left[\zeta(k-\lambda)+\zeta(k+\lambda)\right]\frac{\sin(\lambda s)-\lambda s\cos(\lambda s)}{(\lambda s)^3} \tag{79}$$

When the equation mentioned above is further condensed, it yields,

$$\gamma_4 = \frac{2Hs}{\pi\varepsilon}\int_{-\infty}^{\infty}\left[\zeta(k-\lambda)+\zeta(k+\lambda)\right]\sqrt{\frac{\pi}{2}}\frac{J_{3/2}(\lambda s)}{(\lambda s)^{3/2}}d\lambda \tag{80}$$

where, $J_{3/2}(\lambda s)$ is a first-kind order *3/2* Bessel function. Using the terminal method in references [32, 33] once more, we arrive at

$$\gamma_4 = \left(\frac{2Hs}{\pi\varepsilon}\right)\frac{2}{3s}\zeta(k) = \frac{4H}{3\pi\varepsilon}\zeta(k) \tag{81}$$

Hence, we derive the mechanically displaced element of the FGMEE substrate with a parabolic irregularity at the interfacial surface for EOMO condition as

$$W = \frac{1}{2\pi}\int_{-\infty}^{\infty}\left[\left(\frac{\gamma_1 e^{-r_1 x}}{\gamma\left(1-\dfrac{4H\zeta(k)}{3\pi\gamma\gamma_1}\right)}\right)+\frac{2\gamma}{r_1\gamma_1}e^{r_1 x}e^{-r_1 l}\right]e^{-iky}dk \tag{82}$$

In this situation, the dispersion solution for the SH wave is obtained by

$$\gamma\left(1-\frac{4H\zeta(k)}{3\pi\gamma\gamma_1}\right) = 0 \tag{83}$$

6.4 Frequency equation for parabolically-shaped irregularity at the interfacial surface for ESMS case

The mechanically displaced element of the parabolic-shaped irregular FGMEE substrate in ESMS condition is determined by following the same procedure as in Section 6.3 and using the same asymptotic formulae [32, 33],

$$W = \frac{1}{2\pi}\int_{-\infty}^{\infty}\left[\left(\frac{-2C_{44}^{(01)}e^{-r_1 l}e^{-r_1 x}}{\bar{\gamma}\left(1+\dfrac{2H\zeta'(k)}{3\pi C_{44}^{(01)}e^{-r_1 l}}\right)}\right)+\frac{2}{r_1}e^{r_1 x}e^{-r_1 l}\right]e^{-iky}dk \tag{84}$$

The necessary dispersion solution of the SH wave traveling in parabolic-shaped irregularity, an interfacial surface for the ESMS condition, is given by Eq. (84) as

$$\bar{\gamma}\left(1+\frac{2H\zeta'(k)}{3\pi C_{44}^{(01)}e^{-\eta_1 l}}\right)=0 \qquad (85)$$

7. NUMERICAL CALCULATIONS AND DISCUSSION

In this investigation, we look at four scenarios: a case that is the rectangular-shaped irregularity of EOMO and ESMS cases, and a parabolic-shaped irregularity of EOMO and ESMS cases. A function of wave number is used to describe the influence on the phase velocity of the initial stress. For this study, we consider the magneto-electro-elastic material $BaTiO_3$-$CoFe_2O_4$. The following Table 1 summarizes all of the material constants used in this article.

The effect of the inhomogeneity parameter, depth source, and irregularity on the propagation of plane SH wave in an irregular FGMEE substrate is shown in Figures 3-14. In all the graphs, the dispersion curves have been plotted for phase velocity variation concerning wave number for open and short cases. And also, results are shown for the patients when an irregularity is in the form of a rectangle or a parabola. In general, for all the graphs, the default values of parameters are considered as $\alpha = 0.005, l = 5000, H = 50,$ unless otherwise specified.

7.1 For irregularity in at interface surface with a rectangular form

The graphs for the rectangular-shaped irregularity EOMO case are plotted in Figures 3-5. The relation between phase velocity and wave number is shown in Figure 3 for various inhomogeneity parameter values α(0.0046, 0.0048, 0.005); phase velocity decreases steadily as wave number *k* decreases. For all values of *k*, the phase velocity values drop as *k* increases. For all matters of α, the curves consistently decline and do not cross over. The effect of α is more prominent Figure 4 demonstrates the effect of the relation between phase velocity and wave number for various depth source values *l*(4800, 4900, 5000). It is observed that as the depth source decreases, the phase velocity increases. Figure 5 demonstrates the effect of phase velocity versus wave number for various values of irregularity *H*(50, 60, 70), the nature of the curve is similar to Figure 4.

The graphs for the rectangular-shaped irregularity ESMS case are plotted in Figures 6-8. Figure 6 demonstrates the relation between phase velocity and wave number for various inhomogeneity parameter values α(0.0046, 0.0048, 0.005); the wave number *k* ups and phase velocity progressively comes down for varied α values. For all values of *k*, the phase velocity values increase as α increases. For all deals of α, the curves continuously decline and do not increase. Figure 7 demonstrates the effect of phase velocity versus wave number for various values of depth source *l*(4800, 4900, 5000). For all values of *k*, the phase velocity values increase as *l* increases. This graph exemplifies that the phase velocity rises directly to the rise in *l*. Figure 8 demonstrates the relation between phase velocity and wave number for various irregularity values *H*(50, 60, 70). The graph is similar to the EOMO situation of irregularity.

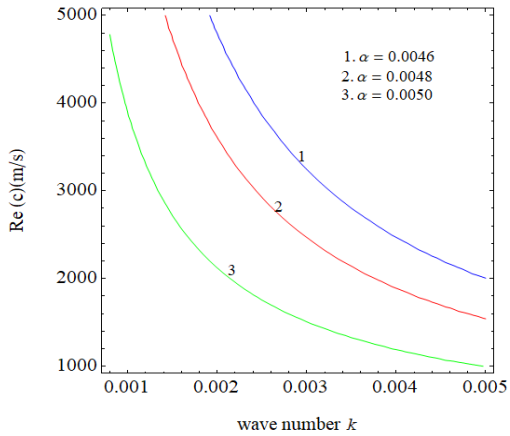

Figure 3. Variations in wave number & phase velocity for the rectangular-EOMO situation with changing values of α

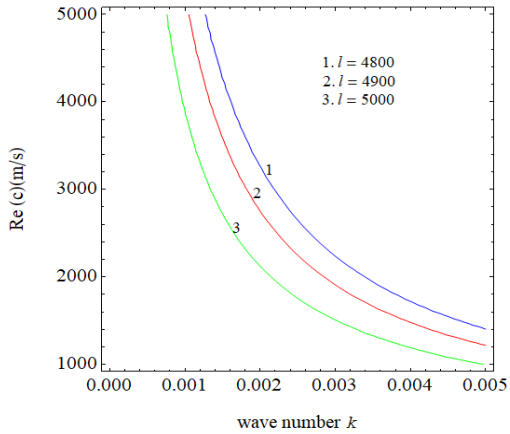

Figure 4. Variations in wave number & phase velocity for the rectangular-EOMO situation with changing values of *l*

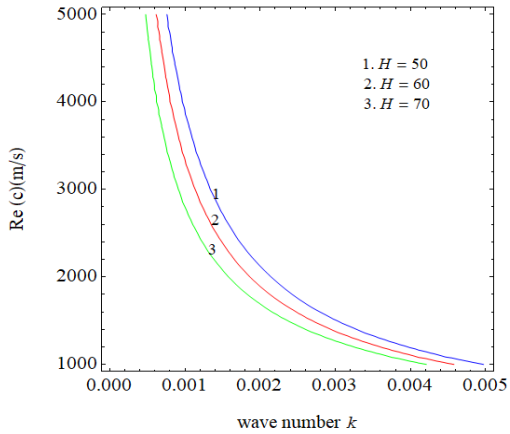

Figure 5. Variations in wave number & phase velocity for the rectangular-EOMO situation with changing values of *H*

Table 1. Material coefficients of the Magneto-electro-elastic substrate $BaTiO_3$-$CoFe_2O_4$

Material	$C_{44}^{(01)}$	$e_{15}^{(01)}$	$h_{15}^{(01)}$	$\mu_{11}^{(01)}$	$\kappa_{11}^{(01)}$	$\beta_{11}^{(01)}$	ρ
$BaTiO_3$-$CoFe_2O_4$	4.8	0.08	238	-258	0.19	0.005	7.5

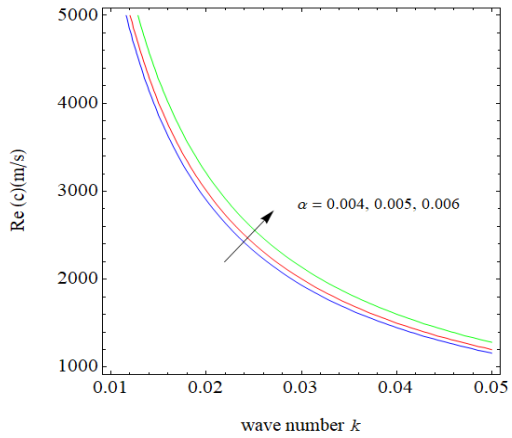

Figure 6. Variations in wave number & phase velocity for the rectangular-ESMS situation with changing values of α

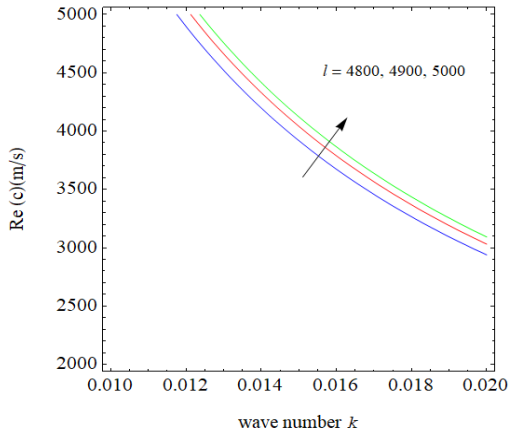

Figure 7. Variations in wave number & phase velocity for the rectangular-ESMS situation with changing values of *l*

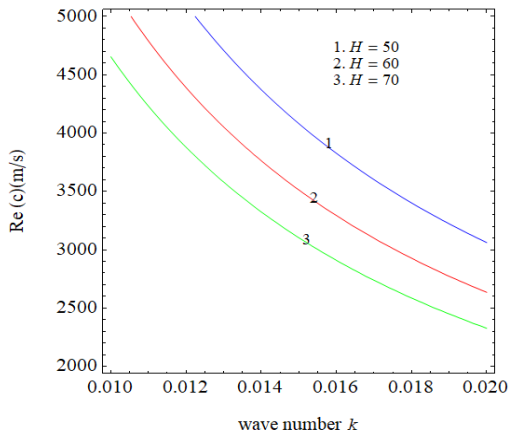

Figure 8. Variations in wave number & phase velocity for the rectangular-ESMS situation with changing values of *H*

7.2 For irregularity in at interface surface with a parabolic form

The graphs for the parabola-shaped irregularity EOMO case are plotted in Figures 9-11. Figure 9 demonstrates the effect of phase velocity with wave number for various values of heterogeneity parameter values α(0.0049, 0.0050, 0.0051). Phase velocity decreases steadily as wave number *k* decreases. For all values of *k*, the phase velocity values drop as *k* increases. For all deals of α, the curves consistently decline and do not cross over. The effect of α is more prominent. Figure 10 demonstrates the effect of phase velocity versus wave number for various values of depth source *l*(4800, 4900, 5000). The impact of the depth source *l* is similar to the α in Figure 9. Figure 11 demonstrates the effect of phase velocity versus wave number for various values of irregularity *H*(50, 60, 70). It is visible that all matters of *H* curves merge. *H* has no effect on the phase velocity of the parabolic EOMO condition.

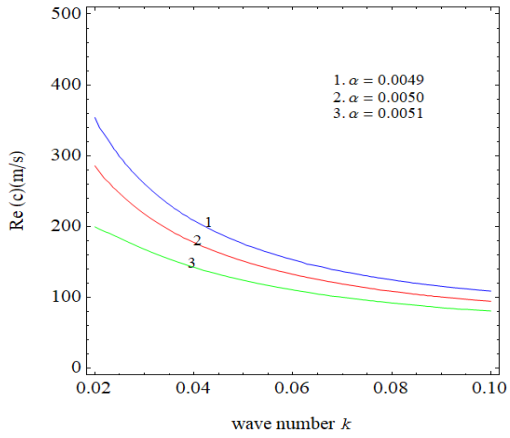

Figure 9. Variations in wave number & phase velocity for the parabolic-EOMO situation with changing values of α

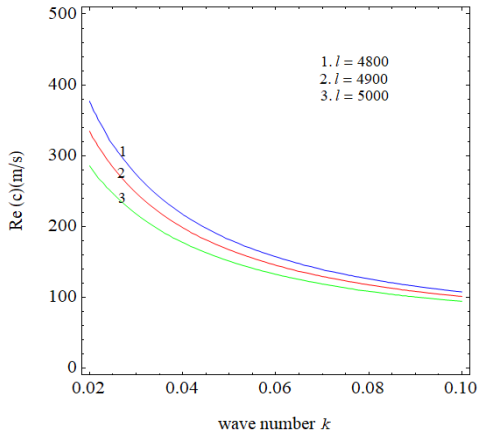

Figure 10. Variations in wave number & phase velocity for the parabolic -EOMO situation with changing values of *l*

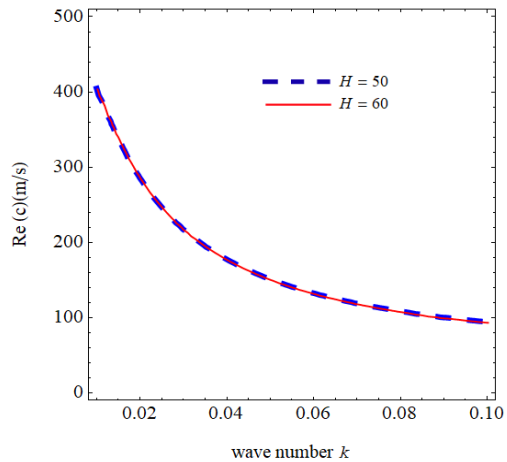

Figure 11. Variations in wave number & phase velocity for the parabolic -EOMO situation with changing values of *H*

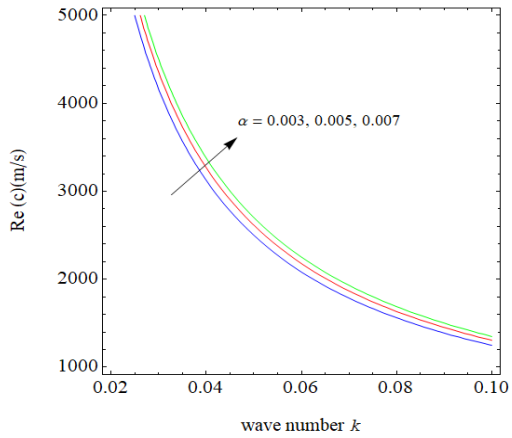

Figure 12. Variations in wave number & phase velocity for the parabolic -ESMS situation with changing values of α

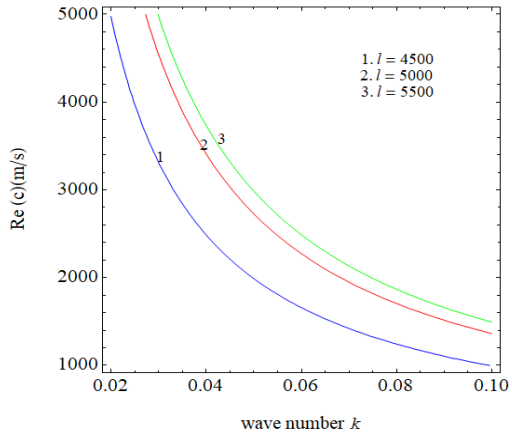

Figure 13. Variations in wave number & phase velocity for the parabolic -ESMS situation with changing values of *l*

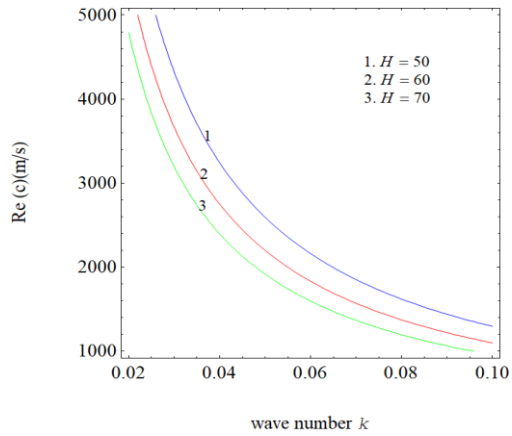

Figure 14. Variations in wave number & phase velocity for the parabolic -ESMS situation with changing values of *H*

The parabolic-shaped irregularity ESMS case graphs are plotted in Figures 12-14. Figure 12 demonstrates the effect of wave number with phase velocity for various α(0.003, 0.005, 0.007) values. The nature of the inhomogeneity parameter α is similar to Figure 6. Figure 13 demonstrates the effect of phase velocity versus wave number for various values of depth source *l*(4500, 5000, 5500). The nature of the depth source *l* is similar to Figure 7. Figure 14 demonstrates the effects of wave number with phase velocity for various irregularity values *H*(50, 60, 70). It is observed that, as the irregularity *H* decreases, the phase velocity increases as *k* increases. The effect of *H* is more prominent in ESMS parabolic conditions.

8. CONCLUSIONS

The present investigation aims to investigate the characteristics of SH waves generated by an impulse point source at the interface between the vacuum and the FGMEE substrate. The dispersion equation's closed-form expression is created using the Fourier series technique. A numerical calculation has shown how the wave number affects the phase velocity of SH waves. Inhomogeneity parameter, depth source, and irregularity related to the FGMEE substrate and vacuum are analyzed and visually depicted for their effects on the propagation properties of SH waves in both open and short situations, of rectangular and parabolic shapes. The following is a summary of the critical elements of the current study:

- With an increase in wave number magnitude, the phase velocity of the SH wave considerably drops.
- In contrast to the other cases (rectangular short and parabolic short), the inhomogeneity parameter causes the phase velocity to increase in both open situations. Comparing open rectangular cases to other cases, it is discovered that the effect is more potent.
- For the two cases (rectangular short and parabolic short), the depth source increases the phase velocity while decreasing the phase velocity in both open situations. Compared to other situations, it is discovered that the effect is more substantial for the short parabolic case.
- The irregularity at the imperfect interface reduces the phase velocity in open and short cases for both rectangular and parabolic. The irregularity strongly affects the phase velocity for all scenarios except the parabolic open condition.
- This calculation model could be the ideal match for laminated FGMEE structures utilized as surface acoustic wave devices since the variation of the film's magneto-electromechanical characteristics changes gradually with depth and throughout the production process (SAW). As a result, it can serve as a theoretical foundation for the design of high-performance SAW devices.

REFERENCES

[1] Van Suchtelen, J. (1972). Product properties: A new application of composite materials. Phillips Research Reports, 27: 28-37.

[2] Van Run, A.M., Terrell, D.R., Scholing, J.H. (1974). An *in situ* grown eutectic magnetoelectric composite material: Part 2 physical properties. Journal of Materials Science, 9: 1710-1714. https://doi.org/10.1007/BF00540771

[3] Bracke, L.P.M., Van Vliet, R.G. (1981). A broadband magneto-electric transducer using a composite material. International Journal of Electronics Theoretical and Experimental, 51(3): 255-262. https://doi.org/10.1080/00207218108901330

[4] Li, J.Y. (2000). Magnetoelectroelastic multi-inclusion and inhomogeneity problems and their applications in

composite materials. International Journal of Engineering Science, 38(18): 1993-2011. https://doi.org/10.1016/S0020-7225(00)00014-8
[5] Liu, J., Liu, X., Zhao, Y. (2001). Green's functions for anisotropic magnetoelectroelastic solids with an elliptical cavity or a crack. International Journal of Engineering Science, 39(12): 1405-1418. https://doi.org/10.1016/S0020-7225(01)00005-2
[6] Pan, E., Han, F. (2005). Exact solution for functionally graded and layered magneto-electro-elastic plates. International Journal of Engineering Science, 43(3-4): 321-339. https://doi.org/10.1016/j.ijengsci.2004.09.006
[7] Bhangale, R.K., Ganesan, N. (2006). Free vibration of simply supported functionally graded and layered magneto-electro-elastic plates by finite element method. Journal of Sound and Vibration, 294(4-5): 1016-1038. https://doi.org/10.1016/j.jsv.2005.12.030
[8] Huang, D.J., Ding, H.J., Chen, W.Q. (2007). Analytical solution for functionally graded magneto-electro-elastic plane beams. International Journal of Engineering Science, 45(2-8): 467-485. https://doi.org/10.1016/j.ijengsci.2007.03.005
[9] Chen, J., Pan, E., Chen, H. (2007). Wave propagation in magneto-electro-elastic multilayered plates. International journal of Solids and Structures, 44(3-4): 1073-1085. https://doi.org/10.1016/j.ijsolstr.2006.06.003
[10] Melkumyan, A. (2007). Twelve shear surface waves guided by clamped/free boundaries in magneto-electro-elastic materials. International Journal of Solids and Structures, 44(10): 3594-3599. https://doi.org/10.1016/j.ijsolstr.2006.09.016
[11] Danoyan, Z.N., Piliposian, G.T. (2008). Surface electro-elastic shear horizontal waves in a layered structure with a piezoelectric substrate and a hard dielectric layer. International Journal of Solids and Structures, 45(2): 431-441. https://doi.org/10.1016/j.ijsolstr.2007.08.036
[12] Li, L., Wei, P.J. (2014). Surface wave speed of functionally graded magneto-electro-elastic materials with initial stresses. Journal of Theoretical and Applied Mechanics, 44(3): 49-64. https://doi.org/10.2478/jtam-2014-0016
[13] Li, L., Wei, P.J. (2014). The piezoelectric and piezomagnetic effect on the surface wave velocity of magneto-electro-elastic solids. Journal of Sound and Vibration, 333(8): 2312-2326. https://doi.org/10.1016/j.jsv.2013.12.005
[14] Wu, C.P., Chen, S.J., Chiu, K.H. (2010). Three-dimensional static behavior of functionally graded magneto-electro-elastic plates using the modified Pagano method. Mechanics Research Communications, 37(1): 54-60. https://doi.org/10.1016/j.mechrescom.2009.10.003
[15] Huang, D.J., Ding, H.J., Chen, W.Q. (2010). Static analysis of anisotropic functionally graded magneto-electro-elastic beams subjected to arbitrary loading. European Journal of Mechanics-A/Solids, 29(3): 356-369. https://doi.org/10.1016/j.euromechsol.2009.12.002
[16] Zhao, L., Chen, W.Q. (2010). Plane analysis for functionally graded magneto-electro-elastic materials via the symplectic framework. Composite Structures, 92(7): 1753-1761. https://doi.org/10.1016/j.compstruct.2009.11.029
[17] Chen, J., Guo, J., Pan, E. (2017). Wave propagation in magneto-electro-elastic multilayered plates with nonlocal effect. Journal of Sound and Vibration, 400: 550-563. https://doi.org/10.1016/j.jsv.2017.04.001
[18] Yang, Z.X., Dang, P.F., Han, Q.K., Jin, Z.H. (2018). Natural characteristics analysis of magneto-electro-elastic multilayered plate using analytical and finite element method. Composite Structures, 185: 411-420. https://doi.org/10.1016/j.compstruct.2017.11.031
[19] Vinyas, M. (2021). Computational analysis of smart magneto-electro-elastic materials and structures: Review and classification. Archives of Computational Methods in Engineering, 28(3): 1205-1248. https://doi.org/10.1007/s11831-020-09406-4
[20] Othmani, C., Zhang, H., Lü, C., Wang, Y.Q., Kamali, A.R. (2022). Orthogonal polynomial methods for modeling elastodynamic wave propagation in elastic, piezoelectric and magneto-electro-elastic composites—A review. Composite Structures, 286: 115245. https://doi.org/10.1016/j.compstruct.2022.115245
[21] Chaki, M.S., Bravo-Castillero, J. (2023). A mathematical analysis of anti-plane surface wave in a magneto-electro-elastic layered structure with non-perfect and locally perturbed interface. European Journal of Mechanics-A/Solids, 97: 104820. https://doi.org/10.1016/j.euromechsol.2022.104820
[22] Chattopadhyay, A., Gupta, S., Sharma, V.K., Kumari, P. (2008). Propagation of SH waves in an irregular monoclinic crustal layer. Archive of Applied Mechanics, 78: 989-999. https://doi.org/10.1007/s00419-008-0209-6
[23] Singh, S.S. (2011). Love wave at a layer medium bounded by irregular boundary surfaces. Journal of Vibration and Control, 17(5): 789-795. https://doi.org/10.1177/1077546309351301
[24] Chattopadhyay, A., Singh, A.K. (2012). Propagation of magnetoelastic shear waves in an irregular self-reinforced layer. Journal of Engineering Mathematics, 75: 139-155. https://doi.org/10.1007/s10665-011-9519-8
[25] Chattaraj, R., Samal, S.K., Mahanti, N.C. (2013). Dispersion of Love wave propagating in irregular anisotropic porous stratum under initial stress. International Journal of Geomechanics, 13(4): 402-408. https://doi.org/10.1061/(ASCE)GM.1943-5622.0000230
[26] Singh, A.K., Kumar, S., Chattopadhyay, A. (2015). Love-type wave propagation in a piezoelectric structure with irregularity. International Journal of Engineering Science, 89: 35-60. https://doi.org/10.1016/j.ijengsci.2014.11.008
[27] Singh, A.K., Chaki, M.S., Chattopadhyay, A. (2018). Remarks on impact of irregularity on SH-type wave propagation in micropolar elastic composite structure. International Journal of Mechanical Sciences, 135: 325-341. https://doi.org/10.1016/j.ijmecsci.2017.11.032
[28] Ray, A., Singh, A.K. (2020). Love-type waves in couple-stress stratum imperfectly bonded to an irregular viscous substrate. Acta Mechanica, 231: 101-123. https://doi.org/10.1007/s00707-019-02525-5
[29] Chaki, M.S., Singh, A.K. (2020). The impact of reinforcement and piezoelectricity on SH wave propagation in irregular imperfectly-bonded layered FGPM structures: An analytical approach. European Journal of Mechanics-A/Solids, 80: 103872. https://doi.org/10.1016/j.euromechsol.2019.103872
[30] Gupta, S., Das, S., Dutta, R. (2021). Case-wise analysis of Love-type wave propagation in an irregular fissured

porous stratum coated by a sandy layer. Multidiscipline Modeling in Materials and Structures, 17(6): 1119-1141. https://doi.org/10.1108/MMMS-01-2021-0003
[31] Chaki, M.S., Singh, A.K. (2021). Scattering and propagation characteristics of SH wave in reduced Cosserat isotropic layered structure at irregular boundaries. Mathematical Methods in the Applied Sciences, 44(7): 6143-6163. https://doi.org/10.1002/mma.7176
[32] Chaki, M. S., Guha, S., Singh, A.K. (2020). Impact of rectangular/parabolic shaped irregularity on the propagation of shear horizontal wave in a slightly compressible layered structure. In Mathematical Modelling and Scientific Computing with Applications: ICMMSC 2018, Indore, India, pp. 61-74. https://doi.org/10.1007/978-981-15-1338-1_5
[33] Singh, A.K., Rajput, P., Chaki, M.S. (2022). Analytical study of Love wave propagation in functionally graded piezo-poroelastic media with electroded boundary and abruptly thickened imperfect interface. Waves in Random and Complex Media, 32(1): 463-487. https://doi.org/10.1080/17455030.2020.1779387
[34] Gupta, S., Dutta, R., Das, S. (2023). Flexoelectric effect on SH-wave propagation in functionally graded fractured porous sedimentary rocks with interfacial irregularity. Journal of Vibration Engineering & Technologies, 22: 1-21. https://doi.org/10.1007/s42417-023-00894-9
[35] Saini, A., Poonia, R.K. (2023). Propagation of love waves under the effect of parabolic irregularity in isotropic fluid-saturated porous medium. Materials Today: Proceedings. https://doi.org/10.1016/j.matpr.2023.02.210
[36] Bhat, M., Manna, S. (2023). Behavior of Love-wave fields due to the reinforcement, porosity distributions, non-local elasticity and irregular boundary surfaces. International Journal of Applied Mechanics, 15(6): 2350042. https://doi.org/10.1142/S1758825123500424
[37] Singh, A.K., Koley, S., Negi, A. (2023). Remarks on the scattering phenomena of love-type wave propagation in a layered porous piezoelectric structure containing surface irregularity. Mechanics of Advanced Materials and Structures, 30(12): 2398-2429. https://doi.org/10.1080/15376494.2022.2053913
[38] Kumari, P., Srivastava, R. (2023). On torsional wave in void type porous layers between viscoelastic and piezoelectric media with parabolic irregularity. Waves in Random and Complex Media, 16: 1-23. https://doi.org/10.1080/17455030.2023.2223687
[39] Willis, H.F. (1948). LV. A formula for expanding an integral as a series. The London, Edinburgh, and Dublin Philosophical Magazine and Journal of Science, 39(293): 455-459. https://doi.org/10.1080/14786444808521694
[40] Tranter, C.J. (1966). Integral Transforms in Mathematical Physics (No. 64). Chapman & Hall.

NOMENCLATURE

T_{ij}	stress tensor
u_i	displacement vector components
D_i	mechanical and electric displacements
B_i	magnetic displacements
C_{ij}	elastic constants (10^{10}N/m^2)
e_{ij}	piezoelectric constants (C/m^2)
μ_{ij}	magnetic permittivity (10^{-6}Ns^{2}C^{-2})
h_{ij}	piezomagnetic constants (N/Am)
β_{ij}	electromagnetic constants (10^{-9}Ns/VC)
S_{ij}	strain tensor
E_i	elastic field intensity
k	wave number
λ	wave length
c	phase velocity
κ_0	vacuum dielectric constant (8.85×10-12F/m)
μ_0	vacuum magnetic permittivity (4π×10-7Ns2C-2)
k_{ij}	Dielectric constants (10-9C/Vm)
H_i	Magnetic field

Greek symbols

ϕ	electrostatic potential
ψ	the magnetic potential
α	functional gradient parameter
η	transform parameter
ϑ	any quantity
ρ	mass density (10^3Kg/m^3)
t	time

Subscripts

(1)	FGMEE substrate
v	vacuum

APPENDIX

$$A_0=\frac{\gamma_1}{\gamma},B_0=\frac{\gamma_2-\mathrm{m}\gamma_1}{\gamma},C_0=\frac{\gamma_3-\mathrm{n}\gamma_1}{\gamma},D_0=\frac{\gamma_2}{\gamma},E_0=\frac{\gamma_3}{\gamma},$$

$$A_1=\frac{\gamma_4}{\gamma},B_1=P_4(k)+\frac{\gamma_5-\mathrm{m}\gamma_4}{\gamma},C_1=P_5(k)+\frac{\gamma_6-\mathrm{n}\gamma_4}{\gamma},D_1=\frac{\gamma_5}{\gamma},E_1=\frac{\gamma_4}{\gamma}.$$

$$\gamma=\left(\overline{C_{44}^{(01)}}r_1-e_{15}^{(01)}r_2\mathrm{m}-h_{15}^{(01)}r_2\mathrm{n}\right)\left\{\left(\kappa_{11}^{(01)}r_1+\kappa_0r_3\right)\left(\mu_{11}^{(01)}r_2+\mu_0r_3\right)\right.$$
$$\left.-\left(\beta_{11}^{(01)}r_2\right)^2\right\}-e_{15}^{(01)}r_2\left\{-\left(\kappa_{11}^{(01)}r_1\mathrm{m}+\beta_{11}^{(01)}r_2\mathrm{n}\right)\left(\mu_{11}^{(01)}r_2+\mu_0r_3\right)\right.$$
$$\left.+\left(\beta_{11}^{(01)}r_1\mathrm{m}+\mu_{11}^{(01)}r_2\mathrm{n}\right)\beta_{11}^{(01)}r_2\right\}+h_{15}^{(01)}r_2\left\{-\left(\kappa_{11}^{(01)}r_1\mathrm{m}+\beta_{11}^{(01)}r_2\mathrm{n}\right)\beta_{11}^{(01)}r_2\right.$$
$$\left.+\left(\beta_{11}^{(01)}r_1\mathrm{m}+\mu_{11}^{(01)}r_2\mathrm{n}\right)\left(\kappa_{11}^{(01)}r_1+\kappa_0r_3\right)\right\}$$

$$\gamma_1=-2C_{44}^{(01)}e^{-r_1l}\left\{\left(\kappa_{11}^{(01)}r_1+\kappa_0r_3\right)\left(\mu_{11}^{(01)}r_2+\mu_0r_3\right)-\left(\beta_{11}^{(01)}r_2\right)^2\right\}$$

$$\gamma_2=2C_{44}^{(01)}e^{-r_1l}\left\{-\left(\kappa_{11}^{(01)}r_1\mathrm{m}+\beta_{11}^{(01)}r_2\mathrm{n}\right)\left(\mu_{11}^{(01)}r_2+\mu_0r_3\right)\right.$$
$$\left.+\left(\beta_{11}^{(01)}r_2\mathrm{m}+\mu_{11}^{(01)}r_2\mathrm{n}\right)\beta_{11}^{(01)}r_2\right\}$$

$$\gamma_3=-2C_{44}^{(01)}e^{-r_1l}\left\{-\left(\kappa_{11}^{(01)}r_1\mathrm{m}+\beta_{11}^{(01)}r_2\mathrm{n}\right)\beta_{11}^{(01)}r_2\right.$$
$$\left.+\left(\beta_{11}^{(01)}r_2\mathrm{m}+\mu_{11}^{(01)}r_2\mathrm{n}\right)\left(\kappa_{11}^{(01)}r_1+\kappa_0r_3\right)\right\}$$

$$\gamma_4 = H_1(k)\left\{\left(\kappa_{11}^{(01)}r_1+\kappa_0 r_3\right)\left(\mu_{11}^{(01)}r_2+\mu_0 r_3\right)-\left(\beta_{11}^{(01)}r_2\right)^2\right\}$$
$$-e_{15}^{(01)}r_2\left\{H_2(k)\left(\mu_{11}^{(01)}r_2+\mu_0 r_3\right)-H_3(k)\,\beta_{11}^{(01)}r_2\right\}$$
$$+h_{15}^{(01)}r_2\left\{H_2(k)\beta_{11}^{(01)}r_2-H_3(k)\left(\kappa_{11}^{(01)}r_1+\kappa_0 r_3\right)\right\}$$

$$\gamma_5 = \left(\overline{C_{44}^{(01)}}r_1-e_{15}^{(01)}r_2\mathrm{m}-h_{15}^{(01)}r_2\mathrm{n}\right)\left\{H_2(k)\left(\mu_{11}^{(01)}r_2+\mu_0 r_3\right)\right.$$
$$\left.-H_3(k)\left(\beta_{11}^{(01)}r_2\right)\right\}-H_1(k)\left\{-\left(\kappa_{11}^{(01)}r_1\mathrm{m}+\beta_{11}^{(01)}r_2\mathrm{n}\right)\left(\mu_{11}^{(01)}r_2+\mu_0 r_3\right)\right.$$
$$\left.+\left(\beta_{11}^{(01)}r_1\mathrm{m}+\mu_{11}^{(01)}r_2\mathrm{n}\right)\beta_{11}^{(01)}r_2\right\}+h_{15}^{(01)}r_2\left\{-\left(\kappa_{11}^{(01)}r_1\mathrm{m}+\beta_{11}^{(01)}r_2\mathrm{n}\right)H_3(k)\right.$$
$$\left.+\left(\beta_{11}^{(01)}r_1\mathrm{m}+\mu_{11}^{(01)}r_2\mathrm{n}\right)H_2(k)\right\}$$

$$\gamma_6 = \left(\overline{C_{44}^{(01)}}r_1-e_{15}^{(01)}r_2\mathrm{m}-h_{15}^{(01)}r_2\mathrm{n}\right)\left\{e_{15}^{(01)}r_2H_3(k)-\beta_{11}^{(01)}r_2H_2(k)\right\}$$
$$-e_{15}^{(01)}r_2\left\{-\left(\kappa_{11}^{(01)}r_1\mathrm{m}+\beta_{11}^{(01)}r_2\mathrm{n}\right)H_3(k)+\left(\beta_{11}^{(01)}r_1\mathrm{m}+\mu_{11}^{(01)}r_2\mathrm{n}\right)H_2(k)\right\}$$
$$+H_1(k)\left\{-\left(\kappa_{11}^{(01)}r_1\mathrm{m}+\beta_{11}^{(01)}r_2\mathrm{n}\right)\beta_{11}^{(01)}r_2\right.$$
$$\left.+\left(\beta_{11}^{(01)}r_1\mathrm{m}+\mu_{11}^{(01)}r_2\mathrm{n}\right)\left(\kappa_{11}^{(01)}r_1+\kappa_0 r_3\right)\right\}$$

$$H_1(k) = P_1(k)-e_{15}^{(01)}r_2P_4(k)-h_{15}^{(01)}r_2P_5(k)$$

$$H_2(k) = P_2(k)-\kappa_{11}^{(01)}r_2P_4(k)-\beta_{11}^{(01)}r_2P_5(k)$$

$$H_3(k) = P_3(k)-\beta_{11}^{(01)}r_2P_4(k)-\mu_{11}^{(01)}r_2P_5(k)$$

$$G_1 = \left\{\left(\kappa_{11}^{(01)}r_1+\kappa_0 r_3\right)\left(\mu_{11}^{(01)}r_2+\mu_0 r_3\right)-\left(\beta_{11}^{(01)}r_2\right)^2\right\}$$
$$\left\{\overline{C_{44}^{(01)}}\left(r_1^2-\alpha r_1\right)A_0-2C_{44}^{(01)}\left(r_1-\alpha\right)e^{-r_1 l}\right.$$
$$\left.+e_{15}^{(01)}\left(r_2^2-\alpha r_2\right)B_0+h_{15}^{(01)}\left(r_2^2-\alpha r_2\right)C_0\right\}$$

$$G_2 = \left\{-e_{15}^{(01)}r_2\left(\mu_{11}^{(01)}r_2+\mu_0 r_3\right)+h_{15}^{(01)}r_2\beta_{11}^{(01)}r_2\right\}$$
$$\left\{-\alpha r_2\kappa_{11}^{(01)}B_0-\alpha r_2\beta_{11}^{(01)}C_0+\kappa_{11}^{(01)}r_2^2B_0\right.$$
$$\left.+\beta_{11}^{(01)}r_2^2C_0-\kappa_0 r_3D_0\right\}$$

$$G_3 = \left\{-\beta_{11}^{(01)}r_2-\kappa_{11}^{(01)}r_1-\kappa_0 r_3\right\}$$
$$\left\{-\alpha r_2\beta_{11}^{(01)}B_0-\alpha r_2\mu_{11}^{(01)}C_0+\beta_{11}^{(01)}r_2^2B_0\right.$$
$$\left.+\mu_{11}^{(01)}r_2^2C_0-\mu_0 r_3E_0\right\}$$

$$G_4 = \left\{e_{15}^{(01)}r_2\left[-\left(\kappa_{11}^{(01)}r_1+\kappa_0 r_3\right)\left(\mu_{11}^{(01)}r_2+\mu_0 r_3\right)\right.\right.$$
$$\left.+\left(\beta_{11}^{(01)}r_2\right)^2+\left(\kappa_{11}^{(01)}r_2\right)\left(\mu_{11}^{(01)}r_2+\mu_0 r_3\right)\right]$$
$$+\beta_{11}^{(01)}r_2\left[\left(\kappa_{11}^{(01)}r_1+\kappa_0 r_3\right)-h_{15}^{(01)}r_2^2\kappa_{11}^{(01)}\right.$$
$$\left.\left.+\beta_{11}^{(01)}r_2\right]\right\}\left\{r_2B_0+r_1\mathrm{m}A_0+r_3D_0\right\}$$

$$G_5 = \left\{-h_{15}^{(01)}r_2\left[\left(\kappa_{11}^{(01)}r_1+\kappa_0 r_3\right)\left(\mu_{11}^{(01)}r_2+\mu_0 r_3\right)\right.\right.$$
$$\left.-2\left(\beta_{11}^{(01)}r_2\right)^2\right]+\mu_{11}^{(01)}r_2\left[\left(\kappa_{11}^{(01)}r_1+\kappa_0 r_3\right)+\beta_{11}^{(01)}r_2\right]$$
$$\left.+e_{15}^{(01)}\beta_{11}^{(01)}r_2^2\left(\mu_{11}^{(01)}r_2+\mu_0 r_3\right)\right\}\left\{r_2C_0+r_1\mathrm{n}A_0+r_3E_0\right\}$$

$$\zeta'(k) = \left\{\overline{C_{44}^{(01)}}\left(r_1-\alpha r_1\right)A_0-2C_{44}^{(01)}\left(r_1-\alpha\right)e^{-r_1 l}\right.$$
$$\left.+e_{15}^{(01)}\left(r_2^2-\alpha r_2\right)B_0+h_{15}^{(01)}\left(r_2^2-\alpha r_2\right)C_0\right\}$$
$$-e_{15}^{(01)}r_2\left(r_2B_0+\mathrm{m}r_1A_0\right)-h_{15}^{(01)}r_2\left(r_2C_0+\mathrm{n}r_1A_0\right)$$